JETIR.ORG ISSN: 2349-5162 | ESTD Year : 2014 | Monthly Issue
JOURNAL OF EMERGING TECHNOLOGIES AND INNOVATIVE RESEARCH (JETIR)
An International Scholarly Open Access, Peer-reviewed, Refereed Journal

Synthesis and Electrochemical Properties of Spinel Cobalt ferrite thin Film Electrode for Supercapacitor Applications

Hanmant Kadam,

[a]Department of Physics, Science college, Nanded

[c]Center for Nanomaterials and Energy Devices, School of Physical Sciences, S. R. T. M.

Abstract:

Herein, we report the structural, morphological characteristics and electrochemical supercapacitor electrode application of Cobalt ferrite thin film electrode, deposited onto stainless-less steel substrate, using electrodeposition method. The X-ray diffraction study corroborates the spinel structure and surface image confirms sponge type morphology. The maximum specific capacitance of 36.37 Fg^{-1} at 10 mVs^{-1} calculated using Cyclic-Voltammetry in 2M NaOH electrolyte.

Keywords: Electrochemical Supercapacitors; electrodeposition; Specific Capacitance; Cyclic-Voltammetry; Spinel Ferrite

Introduction

Cobalt ferrite ($CoFe_2O_4$, CFO) belongs to the family of spinel ferrites. Spinel ferrites (MFe_2O_4, M= Mn, Co, or Ni) are known for their remarkable magnetic, catalytic, optical, and electrical properties [1]. Spinel ferrites including $CoFe_2O_4$, $NiFe_2O_4$, $MnFe_2O_4$, $ZnFe_2O_4$, etc., exhibit interesting magnetic, magneto-resistive, and magneto-optical properties, which can be applied in magnetic fluids [2], biotechnology [3], magnetic recording media [4], absorbing materials [5-6], magnetic resonance imaging fields etc. [7]. Thin films of CFO are used for high temperature gas sensors in literature [8]. However, less attention has been paid on the electrochemical properties of ferrites [9]. Spinel ferrites especially exhibit different red-ox states and have good electrochemical stability [10-11]. Nanoparticles of CFO were synthesized by using various methods including sol-gel [12], solvothermal [13], hydrothermal [14], micellar [15], Langmuir-Blodgett [16], bacterial synthesis [17], and co-precipitation [18] etc., methods. Very few literature reports are known for electrochemical supercapacitive (ES) performance of CFO obtained in thin film form either directly or doctor-blading onto the conducting substrate using electrodeposition method. Kumbhar *et al.* [19] reported the chemical synthesis of nano-flakes of BFO for ES application with SC value as high as 366 F g^{-1}. Deng *et al.* [20] reported the preparation and electrochemical properties of CFO nanorods and

nanorings with conclusion, pure CFO cannot be conductive to satisfactory SC performance. A promising approach to enhance the SC performance is designed based upon novel CFO-based hybrids structures.

Here, in this work, synthesis of CFO structures by using electrodeposition method at room temperature on stainless steel (SS) substrate and their ES applications were explored. Synthesis of CFO thin film, their annealing at 400 ^{o}C, 500 ^{o}C, and 600 ^{o}C temperatures and electrochemical properties were explained. The mechanism of reduction and oxidation from electrolyte was studied from cyclic-voltammetry (CV) measurements. The deposition was carried using potentiostat (Epsilion). The effect of cobalt nitrate and ferric nitrate concentration on structural, morphological, wettability and supercapacitive properties of CFO films have been investigated. The effects of electrolyte concentration and scan rate on SC performance of CFO have also been studied. Additionally, charging-discharging, Raman analysis and impedance characteristics of CFO electrodes were studied.

2. Experimental:

2.1 Electrodeposition set-up for CFO synthesis

Figure 1 covers schematic of experimental set-up used for deposition of CFO films on SS substrate. The working electrode was well-cleaned SS substrates of dimensions 1 x 4 x 0.05 cm^3. The counter electrode was a platinum plate (Pt) of dimensions 1.5 x 4 x 1 cm^3. The reference electrode was an Ag/AgCl. These three electrodes were fitted into a beaker holder having three separate slots for each electrode and the holder was fixed in cylindrical cell containing CFO solution. The deposition of CFO was carried out in galvanostatic mode using chronopotentiometry (CP). All depositions were carried out by using Potentiostat (Epsilion)

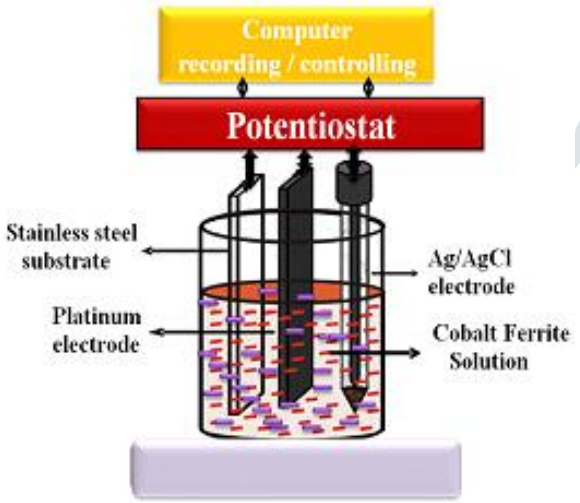

Figure 1: *Schematic experimental set-up for electrodeposition of CFO at room temperature*.

2.2 Substrate cleaning

Substrate cleaning plays an important role in the deposition of thin films. Extremely cleanness of the substrate is required for the deposition as the contaminated substrate surface provides nucleation sites facilitating growth resulting non-uniform films. To investigate supercapacitive performance of thin film electrode, electrically

conducting substrate is the necessary requirement. SS was used as conducting substrates. SS substrates were cleaned according to following procedure;

a) Mirror polished using zero-grade polish paper

b) Washed with detergent and double distilled water

c) Kept in ultrasonication for 15 min and,

d) Finally, dried in stream of argon gas prior to further measurements and used for the deposition.

2.3 Experimental details

All the reagents used in this experiment were of analytical grade, obtained from Aldrich Chemical Co. and used without further purification. CFO films were synthesized in double distilled purified water. The bath was designed from 0.1 M cobalt (II) nitrate ($CO(NO_3)_2.6H_2O$) and 0.2 M ferric (III) nitrate ($Fe(NO_3)_3$) with 0.2 M tartaric acid ($C_4H_6O_6$) as a complexing agent, maintained pH~12 through an addition of sodium hydroxide (NaOH) aqueous solution. Electrodeposition of CFO films onto SS was carried out in galvanostatic mode using CP at 3mA for 300 s. These films were annealed at 400, 500, and 600 ^oC for 2 h.

2.4 Characterization techniques

Crystal structures and phases of the resultant CFO electrodes were confirmed from X-ray diffractometer (XRD) (Rigaku D/MAX 2500 V, Cu Kα, $\lambda = 0.15418$ nm) patterns. Field-emission scanning electron microscopy (FE-SEM, Hitachi S-4200, Korea) digital photoimages were used for morphology confirmation. An Energy-dispersive X-ray spectroscopy (EDX) mapping (Hitachi S-4200, Korea Stereoscan 250 Mk) unit was used for investigation of the elemental composition of the prepared CFO electrodes. For Electrochemical impedance measurement (EIS) impedance analyzer (COMPACTSTATe: IVIUM Switzerland) within a frequency range of 0.001–1.5 MHz with 50 mV amplitude was preferred. Impedance parameters were obtained by fitting the obtained curves using Zview software. Contact angle measurements of as-deposited films were carried out by sessile drop method, in which water drop was observed through a microscope coupled goniometer (Phoenix 150, Surface Electro Optics, Korea). The supercapacitor studies were carried out using the COMPACTSTATe: IVIUM Switzerland where CFO thin film acts as a working electrode, platinum as a counter electrode and Ag/AgCl electrode as a reference electrode. Charge-discharge studies were measured using COMPACTSTATe: IVIUM Switzerlandelectrochemical workstation. Raman analysis is carried out to confirm phase of CFO and bonding.

3. Results and discussion

3.1 Structural studies

The photo images of electrodeposited CFO films onto SS substrate annealed at 400 ^oC, 500 ^oC and 600 ^oC are as shown in Fig.2. Both as-deposited and annealed electrodes were dark black in color; however, electrode annealed at 600 ^0C was reflecting and polished type. Fig. 3 represents typical XRD patterns of CFO electrodeposited at room temperature and air-annealed at 400 ^oC, 500 ^oC and 600 ^oC. All diffraction peaks i.e. (311), (400), (422), (511), (440) were belong to crystal planes of the cubic spinel structure. Major peaks were matching well to that found in JCPDS card no. 22-1086 for spinel ferrite. The cubic spinel structure of CFO was experiencing a space Group: Fd3m (227)

with lattice parameters a= b= c= 8.383 Å which was closely analogous to value found in JCPDS no. 22-1086. From XRD patterns, it was confirmed that CFO film obtained at 500 ^{o}C and 600 ^{o}C annealing temperatures were revealing ferrite form whereas above this temperature sample was peeled off from the supporting substrate i.e. SS whereas below these temperatures spinel phase was uncompleted. From figure it was seen that the CFO obtained at 500 ^{o}C demonstrate dominant peaks compared to 600 ^{o}C annealed sample suggesting that CFO annealed at 500 ^{o}C exhibited better crystallinity than both 400^{o}C, 600 ^{o}C samples.

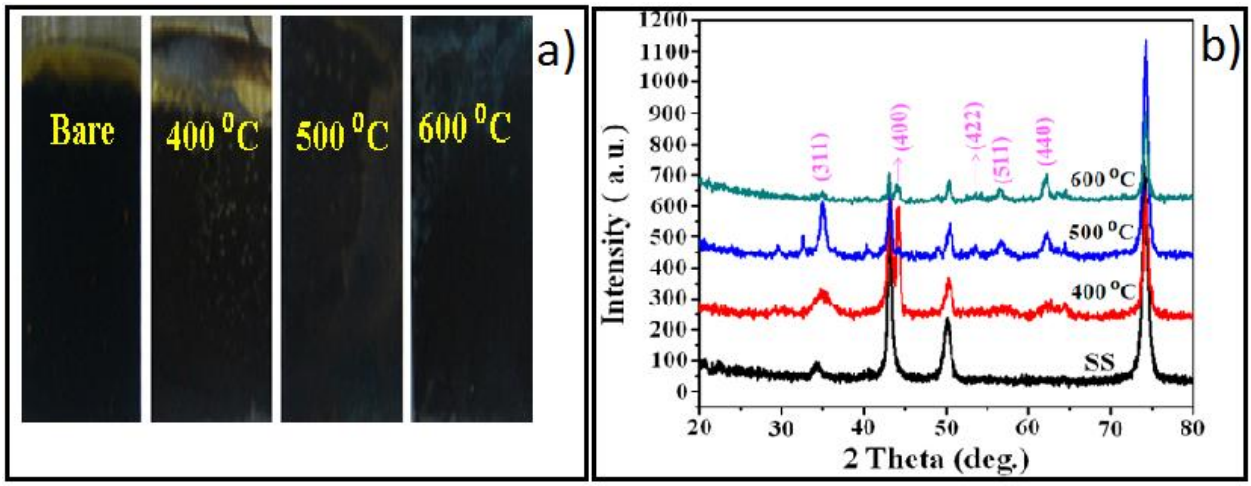

Figure 2: a) *Digital photoimages of pristine and annealed CFO electrodes and b) XRD patterns of annealed CFO films (with XRD of SS).*

3.2 Surface morphology and elemental analysis

After annealing for different temperature FE-SEM image of these products were taken to study their surface morphologies. Fig. 3a), b) and c) shows FE-SEM images of CFO films obtained using electrodeposition method at room temperature on SS substrate and annealed at 400 ^{o}C, 500 ^{o}C, and 600 ^{o}C respectively. At 400 ^{o}C surface morphology of CFO film was rough in nature but crystals were not in similar sizes. As synthesized crystallite were composed of several small spherical crystallites, well agglomerated. After agglomeration resultant crystallites as of island type but was not irregular rather than spherical. There were considerable voids between these islands. After annealing at 600 ^{o}C, CFO surface became relatively porous and fleshy fungi type. Several islands were well merged into one another. It was found that the SC performance of CFO film was maximum when annealed at 600 ^{o}C. Therefore, the same electrode surface was scanned for elemental analysis using EDX. We tried to locate elements like Co, Fe and O over the surface of CFO electrode. Figure 3d) presents EDX spectrum of CFO confirming occurrence presumed elements in desired proportions (1:2:4).

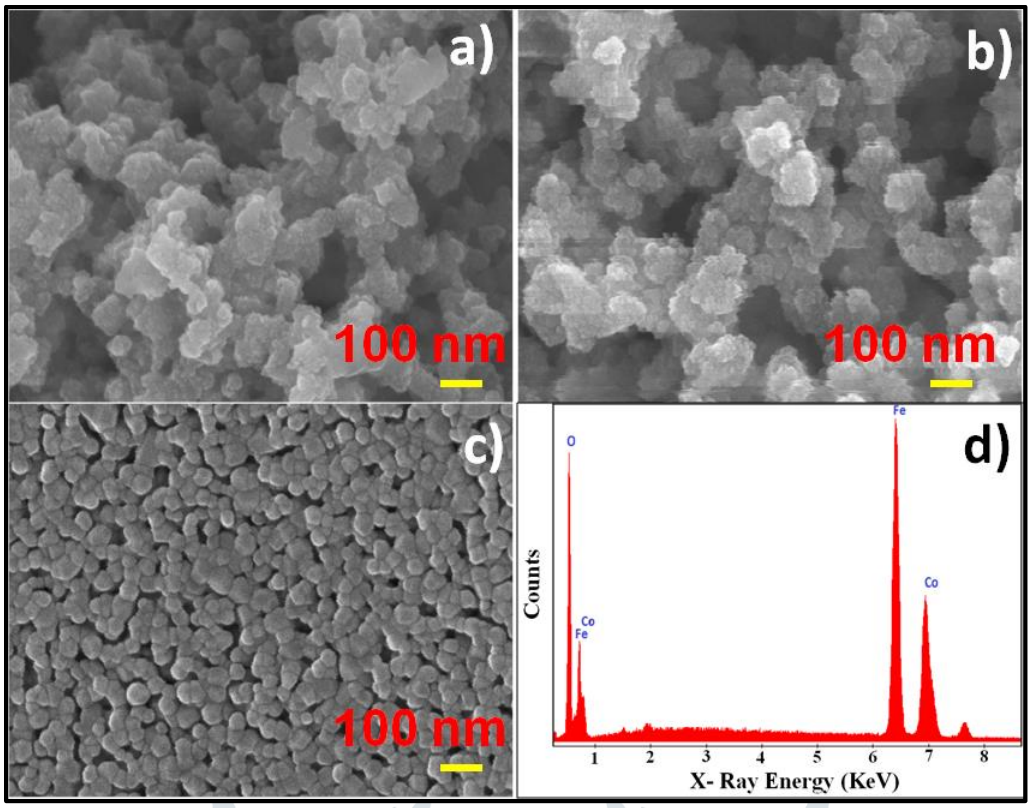

Figure 3: *FE-SEM images of CFO annealed at a) 400 °C b) 500 °C c) 600 °C and d) EDX spectrum for CFO annealed at 600 °C.*

3.3 Raman analysis

Raman spectroscopy is a highly sensitive tool for estimating lattice effects, such as structure transition, lattice distortion, charge-lattice and spin-lattice couplings, local cation distribution, and magnetic ordering etc. Room-temperature Raman spectrums of CFO films obtained under said conditions were scanned in 300-800 cm^{-1} region as shown in Fig. 4. For 400 °C vibrational modes were not detected, hence we have taken Raman of CFO electrodes for 500 °C and 600 °C.

The spectra confirmed single phase formation of the CFO. In spinel ferrite, distribution of divalent and trivalent cations can change due to migration of metal ions from tetrahedral (A) to octahedral (B) sites and *vice-versa.* The obtained poor resolution could be due to overlapping of the peaks corresponding to A and B sites sometimes make the analysis difficult. Group theory predicts the following optical phonon distribution; $5T_{1u}+A_{1g}+E_g+3T_{2g}$; the $5T_{1u}$ modes are IR active [21], whereas other five first order ($A_{1g}+E_g+3T_{2g}$) are Raman active modes [22, 23]. Which are expected for the cubic spinel ferrite system is visible in the spectrum. The $A_{1g}(1)$ mode was due to symmetric stretching of oxygen atoms along Fe-O (or M-O) tetrahedral bonds, E_g and $T_{2g}(3)$ were due to symmetric and asymmetric bending of oxygen with respect to Fe (M), respectively, and T_{2g} (2) was due to asymmetric stretching of Fe (M)-O bond, $T_{2g}(1)$ was due to translational movement of the whole tetrahedron (FeO_4) [24].

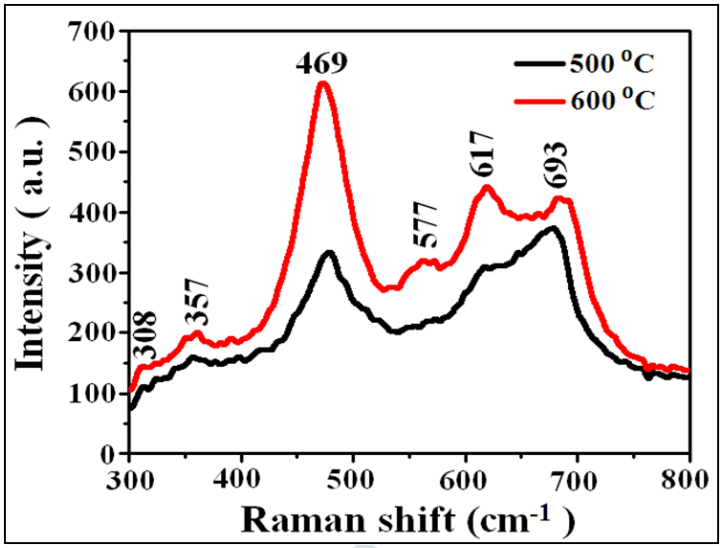

Figure 4: *Raman spectra of CFO electrodes annealed at 500 and 600 ^{0}C temperatures*

In CFO, the octahedral site could be occupied by cobalt and iron ions and the tetrahedral site might be occupied by only the iron ion. Due to the difference in ionic radii of the cobalt and iron ions in CFO, the Fe-O and Co-O bond distances were redistributed between both sites. The modes above 600 cm^{-1} usually represent the motion of oxygen in tetrahedral sub-lattices, and the other low frequency modes were correspond to the vibrational mode of the octahedral sub-lattices. Room temperature Raman spectra at 0.1 M concentration of CO^{2+} ion revealed the presence of six bands in spectrum which basically were broad band's at 308, 357, and 577 cm^{-1}, and strong at 469, 617 and 693 cm^{-1} in the frequency range of 300-800 cm^{-1}.

Raman bands at 693 and 617 cm^{-1} were assigned to $A_{1g}(2)$ and $A_{1g}(1)$ modes that reflected the stretching vibration of Fe^{3+} and O^{2-} ions in octahedral sites (O-site), while low frequency bands at 577, 469, and 308 cm^{-1} were assigned to T_{2g} (3), T_{2g} (2) and E_g modes, respectively, which might cause vibration at the tetrahedral sites (T-site) [25-28]. Raman peak at 469 cm^{-1} was due to the octahedral site mode that reflected the local lattice effect in the octahedral sub-lattice of CFO [29]. The other intense peaks at 617 cm^{-1} and less intense peak at 693 cm^{-1} were due to the symmetry vibrations of the metal in the tetrahedral sites. In addition, at 600 ^{o}C these peaks were relatively sharp with the rise of annealing temperature from 500 ^{o}C, suggesting a harden/completed processes in CFO modes.

3.4 Surface wettability

The contact angle photoimages of SS and CFO surface are shown Fig.5. Surface wettability, an important parameter that enables to know the surface interaction of the metal oxide with given electrolyte, was important measurement during this study.

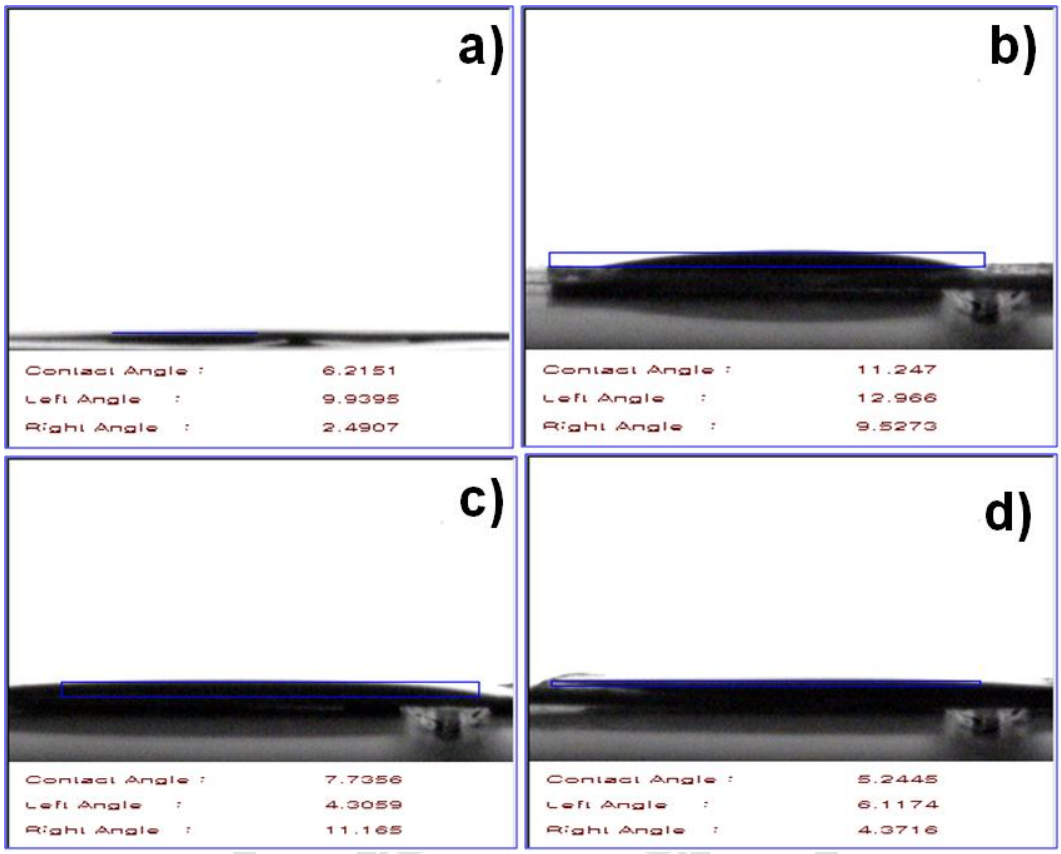

Figure 5: *Contact angle measurements on a) SS and CFO surfaces, annealed at b) 400 ºC, c) 500 ºC, and d) 600 ºC.*

In the present case these values were below 20º indicating super hydrophilic nature of CFO surfaces. On their surface water contact angles were 11º, 7º, and 5º at 400, 500, and 600 ºC annealed temperature respectively. Surface of CFO sample annealed at 600 ºC was similar to that of SS as both are showing nearly same contact values. All surfaces were superhydrophilic. Hydrophilic CFO could be useful for increasing the red-ox reactions rate due to formation of excess Helmholtz-double layer strength caused by relatively strong interfacial contact between electrode and electrolyte [30]. Due to smaller water contact angle value. It was expected that CFO electrode would have superior SC performance than BFO electrode.

3.5 Cyclic-voltammetry

CV measurement is used to explore the CFO anode in a conventional three electrode system for ES performance with different concentration of NaOH electrolyte. The CFO nanostructured electrode prepared at room temperature using three electrode systems were used in the electrochemical supercapacitor application.In CV, electrodeposited CFO films obtained on SS substrate were considered as working electrodes, Ag/AgCl was reference electrode and Pt was counter electrode as shown in Fig.1. The average specific capacitance (SC) was calculated according to calculated according to following equation;

$$SC = I/(mdV/dt) \quad (1)$$

3.6 Electrolytes effect

Room temperature electrodeposited CFO electrodes were used in ES application. ES involves two parts one electrode and second electrolyte. In the present case, CFO film electrodes were tested in different electrolytes for better ES performance including KOH, NaOH, Na_2SO_3, Na_2SO_4, KCl, NaCl etc., and the final electrolyte was chosen wherein ES performance was optimum. CV measurements of CFO electrodes in 2.0 M solutions of; KOH, NaOH, Na_2SO_3, Na_2SO_4, KCl, NaCl were tested in a voltage range of -1000 to +200mV. In all cases, the electrode exhibited symmetric CV characteristics in forward and reverse sweeps (not shown). The NaOH electrolyte offered the largest current among all suggesting fast redo-ox reaction potential in it than others. Hence in rest of the measurements NaOH electrolyte was used. Kumbhar *et al.* [19] reported CFO films electrodes by using chemical synthesis of nano-flakes for ES found to be 366 F g^{-1} NaOH electrolytes. The electrodes annealed at 400 ºC and 500 ºC showed less current density compared to electrodes annealed at 600 ºC which could be due to the formation of ferrite structure at this temperature in contrast to 400 ºC and 500 ºC. But at 600 ºC, current density was relatively higher thereby electrode annealed at 600 ºC was selected in supercapacitor application study.

3.7 Effect of electrolyte concentration

Effect of NaOH electrolyte concentration was studied from 0.25 M to 2.0 M NaOH electrolyte concentration at a scan rate 10 mVs^{-1} within the potential range of -1000 to +200 mV. Fig. 6 revealed effect of NaOH electrolyte concentration on CFO electrodes, electrodeposited at room temperature on SS substrate.

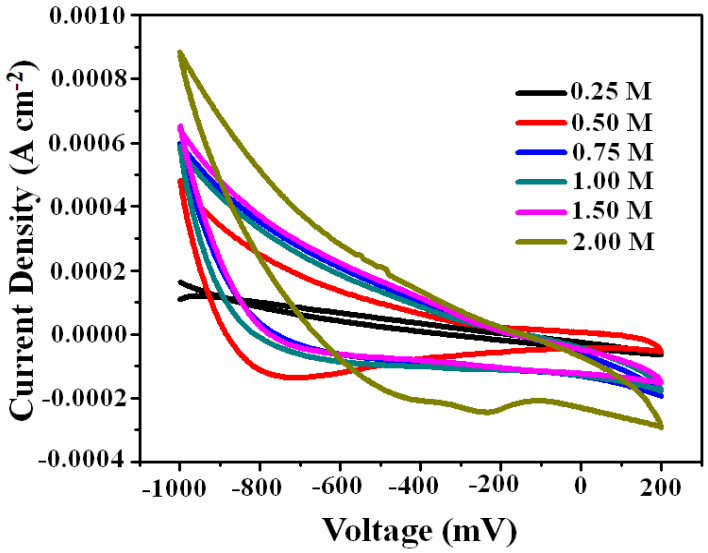

Figure 6: *CV measurements of CFO electrodes (at scan rate of 10 mV s^{-1}) in different concentrations of NaOH electrolyte.*

With increasing concentration of NaOH electrolyte from 0.25 M to 2.00 M, current density under curve was increased.Thereafter, the current density under the curve was fairly constant. It might be due to fact that with increasing concentration of NaOH electrolyte number of Na^+ ions could be increased in electrolyte. Hence with increasing concentration of electrolyte, the ES performance was also increased. When a potential difference is applied across the electrode in a solution, the red-ox reactions occur and the charge is established on the surface of the electrode. Due to the electrostatic interactions, ions in the solution migrate to the electrode to counterbalance the

charge on the electrode, i.e. the Na^+ ions in the present case might travelled from one electrode to the other through the electrolyte during charging and discharging. The movement of electrons occurs at the same time through the current source or through the external load. Thus, the current-voltage profile of the CFOelectrode must be symmetric. In 2M NaOH electrolyte current density was higher compared to other concentrations of NaOH electrolyte. For the higher concentration than 2M NaOH electrolyte, there was no change in the CV curves and current density was almost constant. Hence in 2M NaOH electrolyte CFO showed better performance than that of below 2M NaOH electrolyte concentration. All measured SC values in different concentrations of NaOH electrolyte are listed in Table 1. Thus, maximum obtained SC value was 36.37 Fg^{-1} in 2M NaOH electrolyte.

Table 1: *Effect of NaOH electrolyte concentration on SC values of CFO electrode.*

Electrolyte concentration (M)	0.25	0.5	0.75	1.0	1.5	2.0
Specific capacitance (Fg^{-1})	2.4	20	20.7	21.3	23.2	36.3

3.8 Effects of electrolyte concentration and scan rate

Fig. 10 (a-f) provides CV measurements of CFO film electrodes in; (a) 0.25 M, (b) 0.5 M, (c) 0.75 M, (d) 1.00 M, (e) 1.50 M, and (f) 2.00 M NaOH electrolyte under different scan rates. Voltage range was kept in between -1.0 to + 0.2 V within scan rate range 10, 20, 50, 100, 200, 500, and 1000 mVs^{-1} as shown in Fig. 7 (a-f). As scan rate was increased from 10 to 1000 mVs^{-1} current density also was increased but SC was decreased. At lower scan rate, inner and outer sites of CFO electrodes are active and at higher scan rate, only outer sites are active.Hence at higher scan rate SC was found to be lower and at lower scan rate capacitance was found to be higher. Hence at 10 mVs^{-1} the SC was found to be 36.37 Fg^{-1} and at 1000 mVs^{-1} SC was the least i.e. 1.26 Fg^{-1} in 2M NaOH electrolyte. Fig. 8a) provides an effect of scan rate on SC performance. Details of SC calculated in different scan rate in 2M NaOH electrolyte as given in Table 2. Hence with increasing scan rate the SC value of CFO film electrode was decreased.

Table 2: *Effect of scan rate on SC of CFO electrode.*

Scan rate (mVs^{-1})	**10**	**20**	**50**	**100**	**200**	**500**	**1000**
Specific capacitance (Fg^{-1})	36.37	26.66	13.3	7.82	4.47	1.95	1.26

Figure 7. *CV*

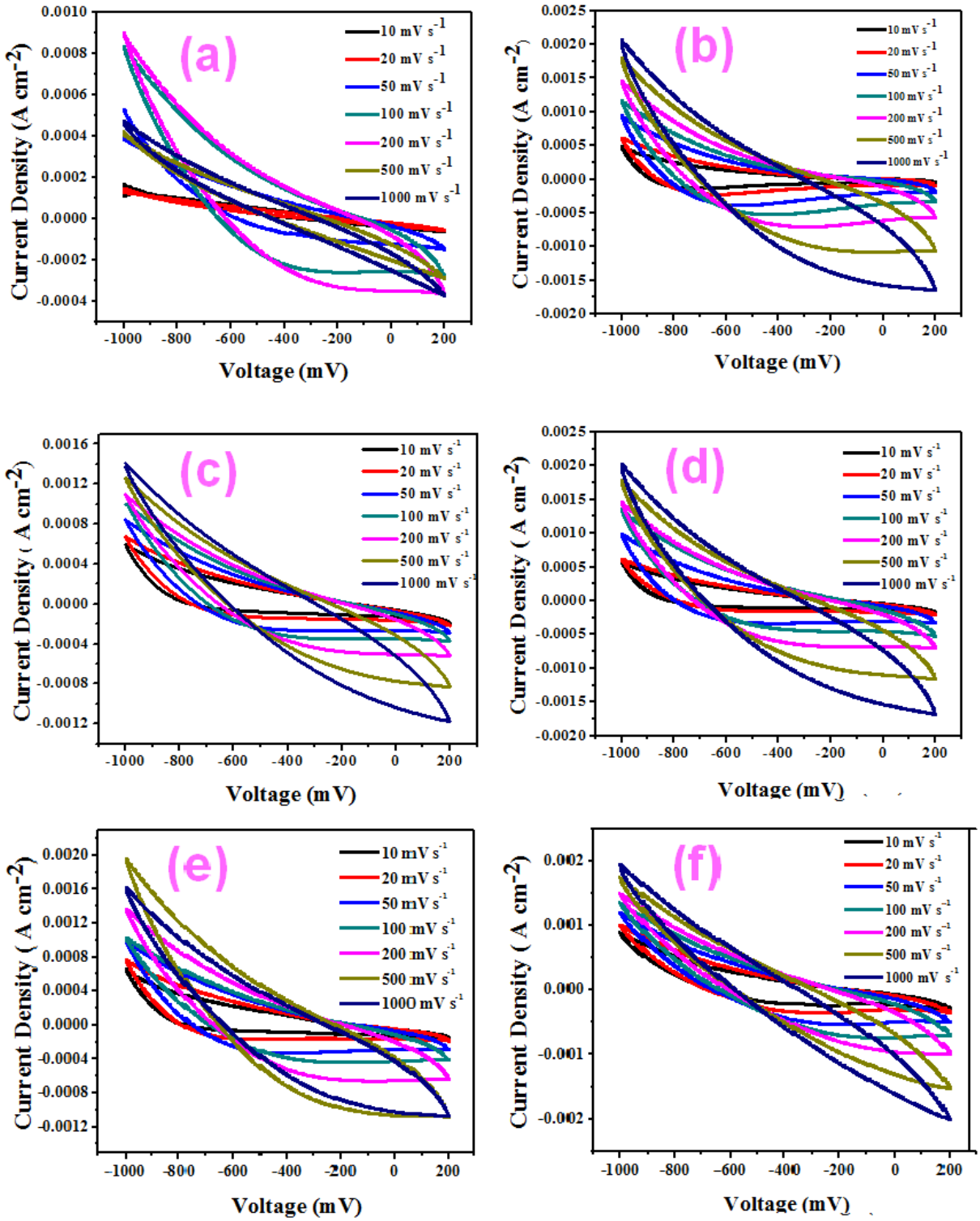

measurements of CFO electrodes under different scanning rates in; (a) 0.25 M, (b) 0.5 M, (c) 0.75 M, (d) 1 M, (e) 1.5 M, and (f) 2 M concentrations of NaOH electrolyte.

Figure 8: a) *Effect of scan rate on SC performance of CFO film electrodes b) Galvanostatic charge-discharge measurements recorded at 1 mA cm^{-2} for the CFO film electrode and c) EIS measurement of CFO electrodein 2M NaOH electrolyte.*

3.9 Galvanostatic charge-discharge studies

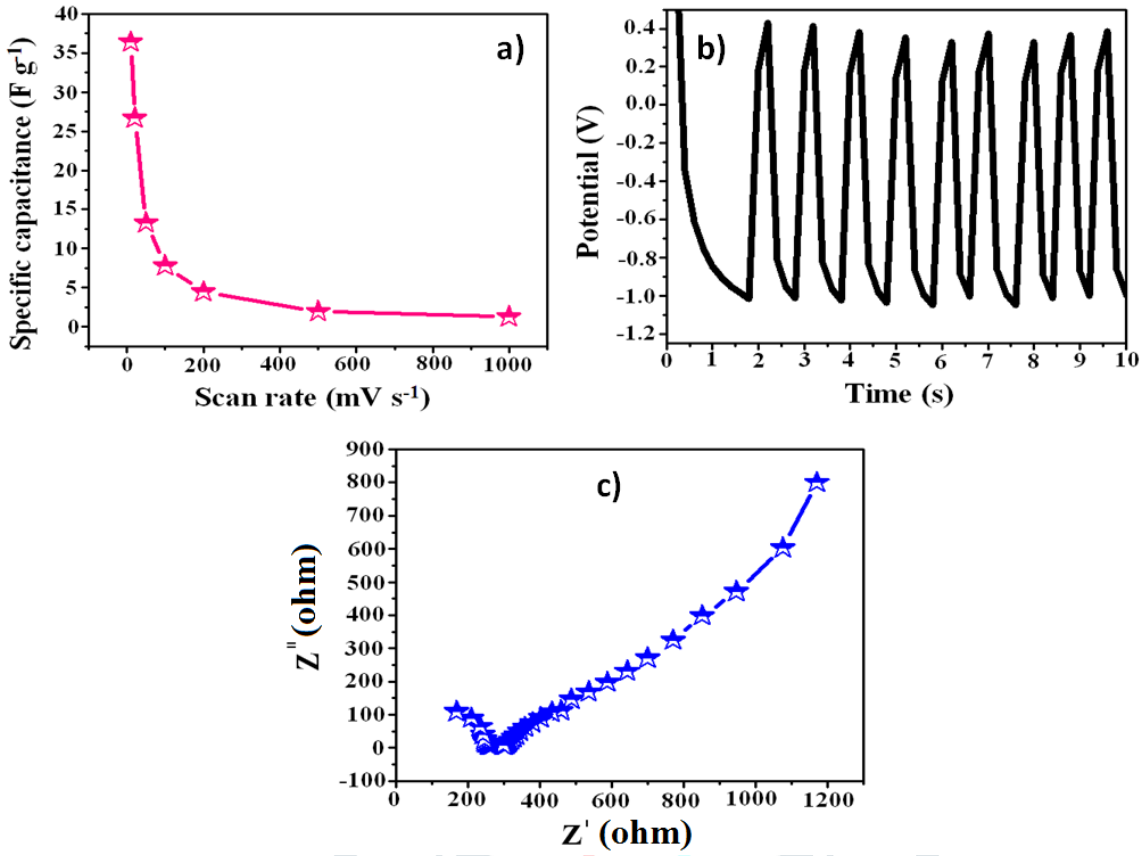

Fig. 8b) shows the charge-discharge curves of a CFO electrode in 2M NaOH electrolyte solution at a current density of 1 mA cm^{-2}.Charge-discharge potential range was kept in between -1.0 to 0.2 V. The charge profile was slightly curved suggesting an ES characteristic. The SE, SP and η (%) of CFO electrode was found to be 0.036 Wh/kg, 0.2 kW/kg and 50 % respectively.

3.10 Electrochemical impedance analysis

In order to investigate the electrochemical characteristics of the supercapacitor electrodes /electrolyte interface in a quantitative manner, AC impedance spectroscopic measurements were performed. Electrochemical impedance spectroscopy measurement of CFO filmelectrodeswas carried out in 2M NaOH electrolyte solution in frequency range 1 mHz to 1 MHz. EIS measurement CFO thin filmelectrodeson SS substrate in 2M NaOH electrolyte is shown in Fig. 8c). It was confirmed from the EIS measurement that the supercapacitor based on CFO demonstrated a very small kinetic arc at high frequencies implying the charge transfer controlled behaviour and a straight line at low frequencies indicating the capacitive behaviour.

4. Conclusions

In summary, here we have demonstrated the electrochemical properties of sponge like $CoFe_2O_4$ spinel ferrite nanostructure. The XRD analysis confirmed the formation of single phase spinel ferrite. SEM micrograph shows porous sponge like structure with micropores that enable transfer of electrolytes ions. The effects of electrolyte concentration and scan rate on SC performance of CFO have also been studied. The electrochemical study exhibit the specific capacitance 36.37 Fg^{-1} at 10 mVs^{-1}.

5. Reference's

[1] S. H. Sun, H. Zeng, D. B. Robinson, S. Raoux, P. M. Rice, S. X. Wang, G. X. Li, Monodisperse MFe_2O_4 (M= Fe, Co, Mn) nanoparticles. J. Am. Chem. Soc. 126 (2004) 273-279.

[2] S. Chikazumi, S. Taketomi, M. Ukita, M. Mizukami, H. Miyajima, M. Setogawa, Y. Kurihara, Physics of magnetic fluids. J. Magn. Magn.Mater. 65 (1987) 245-251.

[3] Y. W. Jun, Y. M. Huh, J. S. Choi, J. H. Lee, H. T. Song, S. Kim, S. Yoon, K. S. Kim, J. Shin S. Cheon, Nanoscale size effect of magnetic nanocrystals and their utilization for cancer diagnosis via magnetic resonance imaging. J. Am. Chem. Soc. 127 (2005) 5732-5733.

[4] D. Chiba, M. Sawicki, Y. Nishitani, Y. Nakatani, F. Matsukura, H. Ohno, Magnetization vector manipulation by electric fields. Nature. 455 (2008) 515.

[5] R. C. Che, L. M. Peng, X. F. Duan, Q. Chen, X. L. Liang, Microwave absorption enhancement and complex permittivity and permeability of Fe encapsulated within carbon nanotubes. Adv. Mater. 16 (2004) 401-405.

[6] M. Fu, Q. Jiao, Y. Zhao, H. Li, Vapor diffusion synthesis of $CoFe_2O_4$ hollow sphere/graphene composites as absorbing materials. J. Mater. Chem. A 2 (2014) 735-744.

[7] Z. Li, L. Wei, M. Y. Gao, H. Lei, One-Pot Reaction to Synthesize Biocompatible Magnetite Nanoparticles. Adv. Mater. 17 (2005) 1001-1005.

[8] I. Sandu, L. Presmanes, P. Alphonse, P. Tailhades, Nanostructured cobalt manganese ferrite thin films for gas sensor application. Thin Solid Films 495 (2006) 130-33.

[9] D. K. Pawar, S. M. Pawar, P. S. Patil, S. S. Kolekar, Synthesis of nanocrystalline nickel–zinc ferrite ($Ni_{0.8}Zn_{0.2}Fe_2O_4$) thin films by chemical bath deposition method. J. Alloys Compd. 509 (2011) 3587-3591.

[10] Y. J. Yang, C. Jiang, S. Chen, N. Wang, P. Yang, M. Liu, Y. Cheng, Direct growth of hierarchical $CoFe_2O_4$ flower-like nanoflake arrays on Ni foam for high performance asymmetrical supercapacitor, Journal of Electroanalytical Chemistry 918 (2022) 116385.

[11] C. D. Lokhande, D. P. Dubal, O. S. Joo, Metal oxide thin film based supercapacitors. Curr. Appl. Phys. 11 (2011) 255-270.

[12] N. C. Pramanik, T. Fujii, M. Nakanishi, J. Takada, Effect of Co^{2+} ion on the magnetic properties of sol–gel cobalt ferrite thin films. J. Mater. Chem. 14 (2004) 3328-3332.

[13] H. Wu, L.Gang, W. Xue, Z. Jiamin, C. Yu, S. Jianlin, Y. Hong, H. He, Y. Shiping. Solvothermal synthesis of cobalt ferrite nanoparticles loaded on multiwalled carbon nanotubes for magnetic resonance imaging and drug delivery. Acta biomaterialia, 7 (2011), 3496-3504.

[14] N. Bao, L. Shen, W. An, P. Padhan, C. H. Turner, A. Gupta, Formation mechanism and shape control of monodisperse magnetic $CoFe_2O_4$ nanocrystals. Chem. Mater. 21(2009) 3458-3468.

[15] C. Cannas, A. Ardu, A. Musinu, D. Peddis, G. Piccaluga, Spherical nanoporous assemblies of iso-oriented cobalt ferrite nanoparticles: synthesis, microstructure, and magnetic properties. Chem. Mater.20 (2008) 6364-6371.

[16] D. K. Lee, Y. H. Kim, Y. S. Kang, P. Stroeve, Preparation of a Vast $CoFe_2O_4$ Magnetic Monolayer by Langmuir–Blodgett Technique. J. Phys. Chem. B 109 (2005) 14939-14944.

[17] V. S. Coker, N. D. Telling, G. V. D. Laan, R. A. D. Pattrick, C. I. Pearce, E. Arenholz, F. Tuna, R. E. P. Winpenny, J. R. Lloyd, Harnessing the extracellular bacterial production of nanoscale cobalt ferrite with exploitable magnetic properties. ACS Nano 3 (2009) 1922-1928.

[18] S. Ayyappan, J. Philip, B. Raj, Solvent polarity effect on physical properties of $CoFe_2O_3$ nanoparticles. J. Phys. Chem. C 113 (2009) 590-596.

[19] V. S. Kumbhar, A. D. Jagadale, N. M. Shinde, C. D. Lokhande, Chemical synthesis of spinel cobalt ferrite ($CoFe_2O_4$) nano-flakes for supercapacitor application. Appl. Surf. Sci. 259 (2012) 39-43.

[20] D. H. Deng, H. Pang, J. M. Du, J. W. Deng, S. J. Li, J. Chen, J. S. Zhang, Fabrication of cobalt ferrite nanostructures and comparison of their electrochemical properties. Cryst. Res. Technol. 47 (2012) 1032-1038.

[21] W. B. White, B. A. DeAngelis, Interpretation of the vibrational spectra of spinels. Spectrochim. Acta A: Molecul. Spectrosco. 23 (1967) 985-995.

[22] R. Gupta, A. K. Sood, P. Metcalf, J. M. Honig, Raman study of stoichiometric and Zn-doped Fe_3O_4. Phys. Rev. B 65 (2002) 104430.

[23] L. V. Gasparov, D. B. Tanner, D. B. Romero, H. Berger, G. Margaritondo, Gasparov, L.V., Tanner, D.B., Romero, D.B., Berger, H., Margaritondo, G. and Forro, L., 2000. Infrared and Raman studies of the Verwey transition in magnetite. Phys. Rev. B 62 (2000) 7939.

[24] G. V. M. Jacintho, A. G. Brolo, P. Corio, P. A. Z. Suarez, J. C. Rubim, Structural investigation of MFe_2O_4 (M= Fe, Co) magnetic fluids. J. Phys. Chem. C. 113 (2009) 7684-7691.

[25] D. Varshney, K. Verma, A. Kumar, Substitutional effect on structural and magnetic properties of $A_xCo_{1-x}Fe_2O_4$ (A= Zn, Mg and x= 0.0, 0.5) ferrites. J. Mol. Struct. 1006 (2011) 447-452.

[26] S. R. Naik, A. V. Salker, S. M. Yusuf, S. S. Meena, Influence of Co2+ distribution and spin–orbit coupling on the resultant magnetic properties of spinel cobalt ferrite nanocrystals. J. Alloys Compd. 566 (2013) 54-61.

[27] M. A. G. Soler, C. C. D. Lima, S. W. D. Silva, T. F. O. Melo, A. C. M. Pimenta, J. P. Sinnecker, R. B. Azevedo, V. K. Garg, A. C. Oliveira, M. A. Novak, P. C. Morais, Aging investigation of cobalt ferrite nanoparticles in low pH magnetic fluid. Langmuir 23 (2007) 9611-17.

[28] S. Jovanovic, M. Spreitzer, M. Tramsek, Z. Trontelj, D. Suvorov, Effect of oleic acid concentration on the physicochemical properties of cobalt ferrite nanoparticles. J. Phys. Chem.C 118 (25) (2014) 13844-13856.

[29] G. Shemer, E. Tirosh, T. Livneh, G. Markovich, Tuning a colloidal synthesis to control Co^{2+} doping in ferrite nanocrystals. J. Phys. Chem. C. 111 (2007) 14334-14338.

[30] H. Aoki, H. Kaneko, N. Hasegawa, H. Ishihara, A. Suzuki, Y. Tamaura, The $ZnFe_2O_4$/(ZnO + Fe3O4) system for H_2 production using concentrated solar energy. Solid State Ionics 172 (2004) 113-116.